Isogeometric analysis: vibration analysis, Fourier and wavelet spectra

Erfan Shafei [a] , Shirko Faroughi[* b]

[a] *Assistant Professor Civil Engineering Faculty, Urmia University of Technology, Urmia, Iran.*

[b] *Associate Professor Mechanical Engineering Faculty, Urmia University of Technology. Urmia, Iran.*

A B S T R A C T

This paper presents the Fourier and wavelet characterization of vibration problem. To determine the natural frequencies, modal damping and mass participation factors of bars, a rod element is established by means of isogeometric formulation. The non-uniform rational Bezier splines (NURBS) is presented to characterize the geometry and the deformation field in isogeometric analysis (IGA). Non-proportional damping has been used to measure the real-state energy dissipation in vibration. Therefore, the stiffness, damping and mass matrices are derived by the NURBS basis functions. The efficiency and accuracy of the present isogeometric analysis is demonstrated by using classical finite element method (FEM) models and closed-form analytical solutions. The frequency content, modal excitation energy and damping are measured as basis values. Results show that the present isogeometric formulation can determine the modal frequencies and inherent damping in an accurate way. Damping as an inherent characteristics of viscoelastic materials is treated in a realistic way in IGA method using non-proportional form. Based on results, k-refinement technique has enhanced the accuracy convergence with respect to other refinement methods. In addition, the half-power bandwidth method gives modal damping for the IGA solution with appropriate accuracy with respect to FEM. Accuracy difference between quadratic and cubic NURBS is significant in IGA h-refinement.

1. Introduction

Hughes *et al.*[1] primarily have developed the isogeometric analysis (IGA) technique for automotive engineering and science applications. Since many researchers are working on new simulation and analytical methods, it is noteworthy to determine the further aspects and

feasibilities of IGA. In IGA method, geometry and deformation field are expressed using Bezier spline (B-spline) functions developed by De Boor [2]. It is notable that B-spline is primarily used for exact expressing of geometry in computer aided design (CAD) tools. The differentiation and continuity limitations existing in finite element method (FEM) shape functions are removed in IGA method. Elements have selectable B-spline order with arbitrary control points. Therefore, accuracy and continuity of B-spline functions can be calibrated without changing the geometry of structure. We can refine the meshing using h-, p-, and k-refinement techniques in the isogeometric formulation which is discussed in detail by Cottrell *et al.*[3].

There exist several research works on the applications and formulation of IGA method in engineering problems. Buffa *et al.*[4] presented studies on the discretization of electromagnetic governing equations using isogeometric field expression, which the results showed the higher accuracy of IGA method than FEM in field problems. Aigner *et al.*[5] presented swept volume techniques and the studies of corresponding parameterizations. Hughes *et al.*[6] presented studies of specific integration rules in IGA method. Knot vector refinement methods used for exact geometry definition are discussed in Bazilevs *et al.*[7]. In addition, Bazilevs *et al.* [8] have conducted detailed work on the isogeometric formulation of fluid-structure interaction (FSI). A novel refinement technique called T-spline refinement is discussed in Dörfel *et al.*[9] studies. Recent studies as Lipton *et al.*[10] are focused on the capability of IGA method in solution of static problems with severe meshing distortions. The numerical experts are usually not familiar with the well-designed and potent procedures of isogeometric technique. Instead, there is little data of the modeling needs in the computational geometry.

The approach developed by Hughes *et al.*[6] is established on NURBS chiefly. They have proposed isogeometric curves to match the exact CAD geometry and then have extended them to constitutive equations using NURBS elements. Subsequent mesh refinements in IGA do not require any further link to the geometry and it can enable prevalent adoption of the method in simulation. The h-, p-, and k-refinement techniques increase the efficiency and robustness of IGA over regular FEM codes. All consequent meshes keep the exact geometry of problem. There is two-stage mapping of PDE integration in IGA, which are Gaussian-to-parametric patches, and parametric patches-to-physical mesh mappings. Therefore, various mesh refinement techniques exist for IGA. Recently, Nguyen *et al.*[11] proposed a very good review of the state of the art of IGA.

Hughes *et al.*[12] studied duality and unified analysis of discrete approximations in structural dynamics and vibration. Wang *et al.*[13] proposed novel higher order mass matrices for isogeometric structural vibration analysis. Recently, Thai *et al.* [14] studied the static, free vibration, and buckling of laminated composite plates using isogeometric approach. Weeger et al. [15] conducted studies on nonlinear vibration of Euler–Bernoulli beams within isogeometric framework. Shojaee *et al.* [16] have been worked on the free vibration analysis of thin plates using NURBS-based isogeometric plate element formulation. Moreover, functionally graded plates are analyzed using higher-order shear deformation theory beside isogeometric geometric description by Tran *et al.* [17]. Further, Thai *el al.* [18] developed a layer-wise deformation theory combined with isogeometric displacement field expression analysis for laminated composite and sandwich plates. Phung-Van *et al.* [19] developed an isogeometric framework for analysis of functionally graded carbon nanotube-reinforced composite plates using higher-order shear deformation theory. Tornabene *et al.*[20] developed a new doubly-curved shell element for

the free vibration application of arbitrarily shaped laminated structures using NURBS-based formulation. NURBS-based isogeometric analysis of buckling and free vibration problems for laminated composites plates with complicated cutouts is conducted by Yu *et al.*[21] using a new simple FSDT theory. Fantuzzi *et al.*[22] developed a strong formulation for isogeometric formulation of thin membranes with general shapes. Yin *et al.*[23] developed an extended NURBS-based formulation for buckling and vibration analysis of imperfect graded plates with internal defects. Dedè, *et al.* [24] analyzed the isogeometric numerical dispersion of two-dimensional elastic wave propagation in continuum. Wang *et al.*[13] developed novel higher order mass matrices for isogeometric structural vibration analysis.

This study is focused on the characteristics of IGA method in vibration problems. Since dynamic response aspects of structures are interest target in mechanical and structural engineering, it is noteworthy to process the response signals in IGA approach. In addition, it is necessary to measure the inherent damping of elastic media to detect the possible difference between FEM and IGA methods. However, primarily, the application of isogeometric formulation in vibration problem are presented here, which has frequent use in simulation of dynamic systems. Application of current study can be stated as measurements of numerical isogeometric response in vibration problems. In addition, modal and time-history characteristics of a vibration problem is extended in the framework on isogeometric analysis. IGA Results can be extended into complex cases with lower computational cost than classical FEM. This paper provides a numerical code for the expression and numerical formulation of PDEs in one-dimensional dynamics. In current research framework, the isogeometric approach to evaluate the forced vibration and response measures of elastic and non-prismatic rods is also extended. The IGA formulation of one-dimensional viscoelastic motion is developed and the simulation procedure is implemented in current study. In advance, we test the efficiency of IGA using Fourier and wavelet spectra. The convergence rate of dynamic characteristics is verified by using h-, p- and k-refinement strategies versus FEM and exact solution. In conclusion, the IGA vibration solutions are provided as prospect reference solution.

2. Isogeometric analysis using NURBS

2.1. Knot vector and B-Spline Basis-Function

NURBS are non-uniform rational expression of B-splines and can capture the irregularities in mesh and geometry efficiently. Classic elements in FEM are replaced by "patches" in IGA method, which are in parametric space. Patches define the basis of physical elements in IGA. However, the geometry and material are uniform in parametric space, dissimilar to FEM. If we want to generate n number of B-spline basis functions with p order (degree), one needs to generate a knot vector. A one-dimensional knot vector is the set of coordinates in the parametric space with $\Xi = \{\xi_1, \xi_2, \cdots, \xi_{n+p+1}\}$ expression[1]. The ξ_i term is the coordinate of ith knot, which has a real value. Nodes are interpolatory at the ends of element intervals. However, the basis-functions generated by the knots are only interpolatory at the ends of the parametric space interval, $\{\xi_1, \xi_{n+p+1}\}$, if the knot vector is open. A knot vector is open if the first and last knots appear $p+1$ times. Therefore, several knots can be placed at the same coordinate in the parametric space, dissimilar to the nodes in FEM. The basis-functions generated by the open knot vectors are not generally interpolatory at interior knots. Given a uniform open knot vector, B-spline basis functions are recursively explained starting with $p=0$ as Eq. (1)[2].

$$N_{i.0}(\xi) = \begin{cases} 1 & \text{if } \xi_i \leq \xi < \xi_{i+1} \\ 0 & \text{otherwise} \end{cases} \tag{1}$$

For p ≥ 1, the B-splines are defined as Eq. (2) [2].

$$N_{i.p}(\xi) = \frac{\xi - \xi_i}{\xi_{i+p} - \xi_i} N_{i.p-1}(\xi) + \frac{\xi_{i+p+1} - \xi}{\xi_{i+p+1} - \xi_{i+1}} N_{i+1.p-1}(\xi) \tag{2}$$

The derivatives of functions with respect to ξ can be calculated using standard techniques. The main difference between FEM shape functions and B-spline basis functions is described as Eq. (3) [2].

$$\forall \xi \in \Xi \rightarrow \begin{cases} \sum_{i=1}^{n} N_{i.p}(\xi) = 1 \\ N_{i.p}(\xi) \geq 0 \end{cases} \tag{3}$$

While the summation of FEM shape functions is unit only in nodes, B-splines have the unity summation over every coordinate in the parametric space patch. In addition, each basis function is not negative unlike the FEM interpolators. Therefore, the terms of constitutive matrixes (stiffness, mass, and damping) are not calculated as negative. This shows the superior aspect of IGA method in computational mechanics which is not treated as well in the FEM. The NURBS curves and the related first-order derivatives for the arbitrary Ξ open knot vector with $p = 2$ are demonstrated in Figure 1. The length of knot vector is $n + p + 1$, which n is the basis-function numbers.
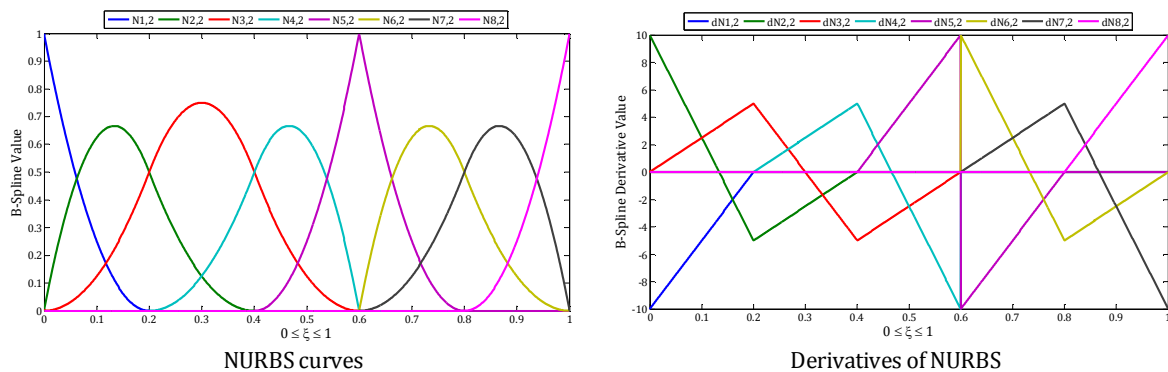

Fig 1: NURBS and derivatives for $\Xi = \{0, 0, 0, 1/5, 2/5, 3/5, 3/5, 4/5, 1, 1, 1\}$ open, non-uniform knot vector

One may express the geometry of physical domains using the linear combination of NURBS basis-functions. Each basis-function is multiplied by control point coordinate to generate the geometry. Control points in IGA have the analogous sense as the nodes in FEM. It should be noted that geometry curve has the same continuity of B-spline basis-functions. The isogeometric geometry is expressed as Eq. (4) for n number of control points[2] .

$$X(\xi) = \sum_{i=1}^{n} N_{i.p}(\xi) X_i \tag{4}$$

The isogeometric geometry is C^{p-1} continuous in non-repeated knots and C^0 continuous in repeated knots, which is also shown in Figure 1. We now explain the refinement methods, which are used to measure the accuracy and validity of IGA meshing. The first technique is knot insertion, called as h-refinement. Such as, we can refine the knot vector $\Xi_1 = \{0,0,0,1,1,1\}$ with

n = 3 to $\Xi_2 = \{0,0,0,1/2,1,1,1\}$ with $n = 4$ without change in curve order. Second approach is the order raise of NURBS, called as p-refinement. It is the case that we change the knot vector $\Xi_1 = \{0,0,0,1,1,1\}$ with $p = 2$ to $\Xi_2 = \{0,0,0,0,1,1,1,1\}$ with $p = 3$. We should note that the multiplicity of knots and the numbers of control points are increased. Although the location of control points is changed in p-refinement, the order-elevated geometry is identical to the preliminary geometry. The third technique is the order elevation followed by the knot insertion, called as k-refinement approach. For example, we have k-refined if we change the $\Xi_1 = \{0,0,0,1,1,1\}$ knot vector to the $\Xi_2 = \{0,0,0,0,1/2,1,1,1,1\}$ ordered and elevated knot vector. So, growth in the number of control points is limited in this case. In addition, the continuity of derivatives of NURBS is preserved in knot insertion stage. Figure 2 shows all the refinement methods.
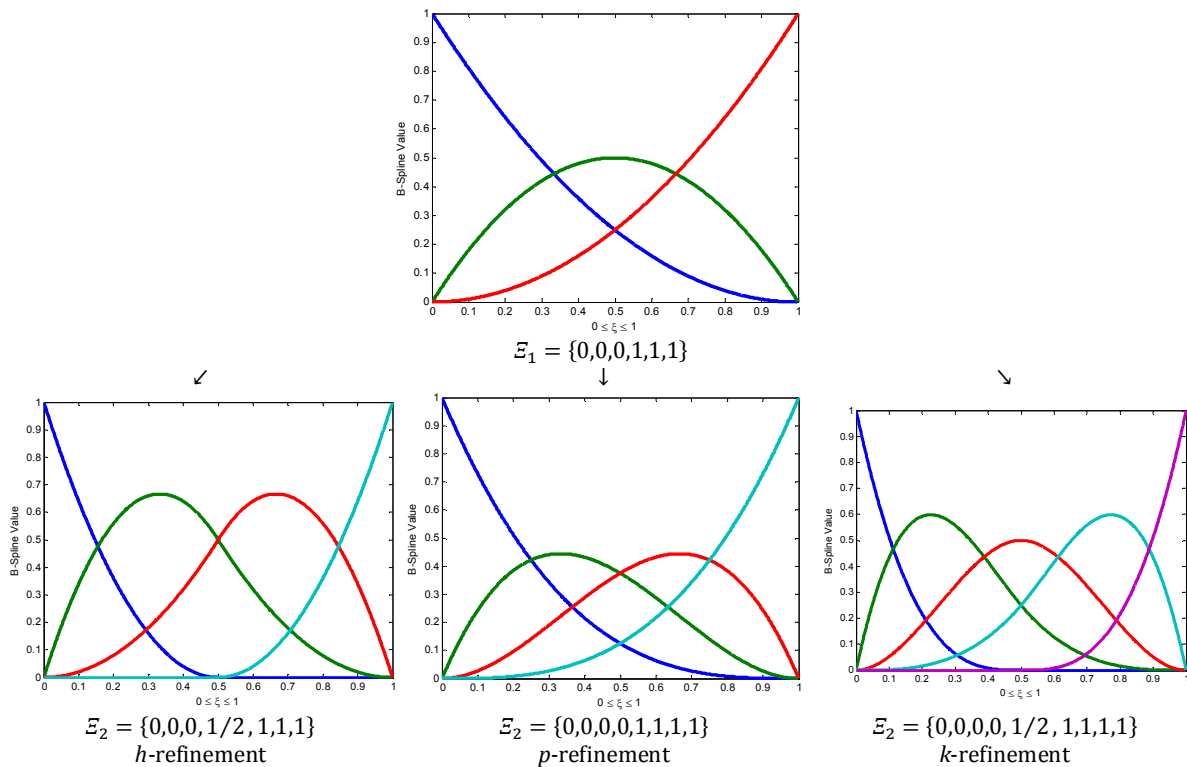

Fig 2: Refining techniques in isogeometric formulation

The advantages of each technique will be discussed in analysis section of current study in the response measurements of simulated system. One has to go through each method and present the sequential results if they are used in isogeometric analysis of vibration problems. Now one needs to define the NURBS and establish the governing equations in isogeometric framework. For this purpose, this paper primarily present the rational or weighted form of basis-functions and the NURBS as Eq. (5) and (6), respectively[2].

$$R_i^p(\xi) = \frac{N_{i,p}(\xi)w_i}{\sum_{j=1}^n N_{j,p}(\xi)w_j} \tag{5}$$

$$C(\xi) = \sum_{i=1}^n R_i^p(\xi)C_i \tag{6}$$

149

In above relation, C_i can be any arbitrary quantity in i^{th} control point (coordinate, displacement, velocity, acceleration, etc.) which are interpolated using NURBS (R_i^p). It is clear that the continuity of NURBS basis-functions are analogous to the NURBSs. Now we can use the NURBS as the basis for wave-propagation simulation. However, there is a need to define the element in isogeometric concept. In one-dimension problems, Hughes *et al.* [1] defined the IGA element as the distance between two individual knots. Consequently, the number of elements is the number of non-zero knot spans in the knot vector Ξ. In IGA, meshing is the patch of knot vector and the control points related with the NURBS outline the geometry. Dissimilar to the FEM, elements have overlaps in IGA and the governing equations are formulated in the whole domain of problem. Therefore, the assembled form of constitutive matrixes in IGA is completely different from those obtained in the FEM. Since the continuity of NURBS are easy to deal with in the isogeometric formulation, there is no severe jumps of field values and it is one of the several advantages of the IGA method.

2.2 Isogeometric Kinematics and Equilibrium

In this section, we establish the governing equations and the discretization using isogeometric element (IGE) to introduce the geometry and displacement field in terms of the control point value x_i as Eq. (7).

$$x(\xi) = \sum_{i=1}^{n} R_i^p(\xi) x_i \tag{7}$$

We should highlight that in the motion, control points and isogeometric elements move with the material particles with which they were initially associated (Lagrange formulation). Therefore, we describe the motion in terms of the instantaneous position of control points. Likewise, restricting the motion caused by an arbitrary growth u to be consistent with above relation suggests that the displacement will be as Eq. (8) [3]:

$$u(x) = \sum_{i=1}^{n} R_i^p(x) u_i \tag{8}$$

We can define the linear strain as Eq. (9)[3]:

$$\epsilon = \frac{1}{2} \sum_{i=1}^{n} \left(u_i \otimes \frac{\partial}{\partial x} R_i^p + \frac{\partial}{\partial x} R_i^p \otimes u_i \right) \tag{9}$$

Ahead, we obtain NURBS mesh gradient using the derivatives of the patch domain as Eq. (10)[3]:

$$\frac{\partial}{\partial x} R_i^p(x) = \left(\frac{\partial x}{\partial \xi} \right)^{-1} \frac{\partial}{\partial \xi} R_i^p(\xi) \tag{10}$$

In numerical analysis, we need to discretize the spatial equilibrium equations in the matrix-vector representation. This needs a retreat of constitutive law for viscose-elastic material as Eq. (11)[6]:

$$\sigma = E\epsilon + \mu\dot{\epsilon} \tag{11}$$

where E is the elastic modulus, ϵ is axial strain, μ is the inherent viscosity and $\dot{\epsilon}$ is the strain rate. The Eq. 11 is Kelvin-Voigt viscoelastic model, which is the typical model used for classic purposes and not a general constitutive law for all kinds of viscoelastic materials. This model is used to demonstrate the effect of inherent damping in modal and transient response beside energy dissipation rate of the system when it is modeled in isogeometric framework. Strain consistency can be expressed in terms of the typical B matrix and the control point displacements as Eq. (12) [3]:

$$\epsilon = \sum_{i=1}^{n} B_i(x)u_i \rightarrow B_i(x) = \frac{\partial}{\partial x} R_i^p(x) \tag{12}$$

Now we combine constitutive and strain consistency to calculate the internal stress. In advance, we can discretize the total virtual work equation [3] to be rewritten as Eq. (13) if the virtual displacement of control point a with i knot index.

$$\delta W(\delta u_a) = \delta W_c(\delta u_a) + \delta W_i(\delta u_a) - \delta W_f(\delta u_a) \tag{13}$$

Note that the formulated internal virtual work includes terms as δW_c and δW_i which denote constitutive and inertial terms. External virtual work includes the δW_f term that expresses the body force effect. The constitutive component of the internal virtual work can now be rewritten in matrix form as Eq. (14) which relating the displacements of control points a and b [6].

$$\delta W_c = \delta u_a^T A \int_L \{B_a^T E B_b u_b + R_a^T \mu R_b \dot{u}_b\}dx = \delta u_a^T K_{ab} u_b + \delta u_a^T C_{ab} \dot{u}_b \tag{14}$$

The K_{ab} and C_{ab} terms denotes the stiffness and damping matrixes of rod element, respectively formulated in IGA. In addition, A is the cross section and L is the length of IGE. Inertial part of the external virtual work is expressed in matrix form as relating the virtual displacement of control point a and acceleration of control point b in order as Eq. (15) [6].

$$\delta W_i = \delta u_a^T A \int_L \{R_a^T \rho R_b \ddot{u}_b\}dx = \delta u_a^T M_{ab} \ddot{u}_b \tag{15}$$

The ρ term is unit density per area of material. The body force, f, is independent of the motion and consequently is constant regarding deformation of media. Thus, the virtual external work due to applied body force per isogeometric element can be expressed in vector form as Eq. (16) [6]:

$$\delta W_f = \delta u_a^T A \int_L \{R_a^T f\}dx = \delta u_a^T f_a \tag{16}$$

Here, the f_a term is the external equivalent forces in control point a. Regarding acquired terms in matrix set of equation, governing equilibrium is independent of the arbitrary displacement assumed for a control point and therefore will have the form as expressed in Eq. (17):

$$K_{ab} u_b + C_{ab} \dot{u}_b + M_{ab} \ddot{u}_b = f_a \tag{17}$$

Regardless of which configuration is used for parametric patch, the resulting displacement, velocity and acceleration vectors will be identical in isogeometric analysis. It is, however, usually easy to initiate the discretized quantities in the spatial knot arrangement. Rewriting the relations of all control point leads into Eq. (18) matrix form.

$$Ku + C\dot{u} + M\ddot{u} = f \qquad (18)$$

For free vibration analysis, governing equation will have Eigenvalue form as Eq. (19) where ω_n is the vector containing natural angular frequencies of system [6].

$$M^{-1}K - I \cdot \omega_n^2 = 0 \qquad (19)$$

In order to solve the set of equations, we need a numerical integration algorithm used in elastodynamics. We choose the explicit time integration using central difference method which is used mainly for vibration problems. It is called explicit method because the equilibrium equation is used at time t to obtain the solution for time $t + \Delta t$. Using central difference approximation of acceleration and velocity vectors would modify above equilibrium at time t as Eq. (20)[6] :

$$Ku_t + C\{u_{t+\Delta t} - u_{t-\Delta t}\}\frac{1}{2\Delta t} + M\{u_{t+\Delta t} - 2u_t + u_{t-\Delta t}\}\frac{1}{\Delta t^2} = f_t \qquad (20)$$

By this substitution, the displacement vector in $t + \Delta t$ increment is an explicit function of two previous t and $t - \Delta t$ increments status. Rearranging Eq. (20) will present statement as Eq. (21) [6]:

$$u_{t+\Delta t} = \left(M + C\frac{\Delta t}{2}\right)^{-1}\left\{(f_t - Ku_t)\Delta t^2 + 2Mu_t - \left(M - C\frac{\Delta t}{2}\right)u_{t-\Delta t}\right\} \qquad (21)$$

We need a starting displacement vector, u_1, is acquired as Eq. (22) or initialization of solution algorithm [6].

$$u_1 = M^{-1}\left\{(f_0 - Ku_0)\frac{\Delta t^2}{2} + \left(M - C\frac{\Delta t}{2}\right)\dot{u}_0\Delta t\right\} + u_0 \qquad (22)$$

Limited available information about inherent damping of structures subjected to dynamic loads made to assume a proportional Rayleigh damping in terms of mass and stiffness matrixes. However, viscosity is the intrinsic property of material and therefore we need to express it in the non-proportional form. We assume various values for inherent viscosity and measure the modal damping ratio based on the Fourier spectrum characteristic in advance.

3. Numerical simulation

In this section, we go through numerical models to check the validity and accuracy of IGA method in modeling of the vibration. We check the sensitivity of dynamic response characteristics to the element size and the refinement technique used. Primarily, we validate the vibration frequencies of response for various refinements and then we assess the characteristics of dynamic response using Fourier and wavelet spectra. In advance, we will measure the excitation and dissipated energy in time domain. We select the cantilever and clamped rod members with impulsive force excitation. In addition, the numerical code is developed in $MATLAB^{®}$ [25]environment and the parallel processing algorithm is used for analysis threading.

3.1. Modeling and oscillation analysis

This paper assume a clamped rod with elastic modulus (E) of $200\ GPa$, section area (A) of $78.54\ mm^2$, length (L) of 3000 mm and mass density (ρ) of $7.85 \times 10^{-9}\ ton/mm^3$. The geometry and isogeometric meshing of the member is show in Figure 3. The size of physical

152

elements is uniform along the member to regularize the integration procedure. We primarily get the frequencies and check their accuracy.
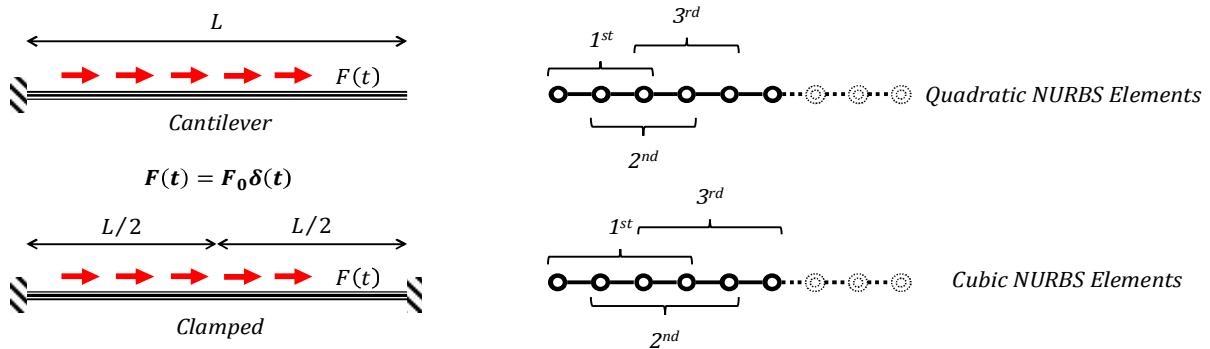

Fig3: Geometry and isogeometric meshing of member regarding quadratic and cubic NURBS elements

The authors use all the refining techniques in isogeometric formulation to investigate the efficiency of each method used. The analytical values of vibration frequencies of cantilever and clamped rods are as Eq. (23) and (24), respectively[2] .

$$\omega_n = \frac{(2n-1)\pi}{2} \frac{\pi}{L} v_c \tag{23}$$

$$\omega_n = n \frac{\pi}{L} v_c \tag{24}$$
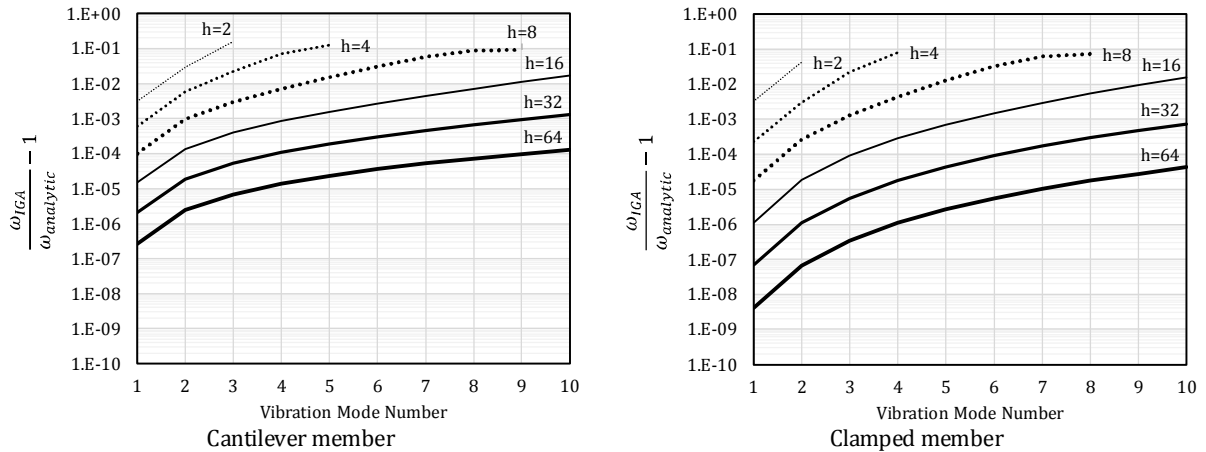
Fig 4: Relative estimation error for quadratic NURBS in h-refining

The v_c term is the longitudinal stress wave velocity and equals to $\sqrt{E/\rho}$. We start with the h-refinement technique that is close to the physical mesh refinement in FEM. In addition, we use quadratic and cubic NURBS basis-function for definition of the geometry and displacement field. The initial knot vector used for mesh generation ($h = 1$) is $\Xi_1 = \{0,0,0,1,1,1\}$ which has only one quadratic isogeometric element. We generate the mesh by means of bisecting isogeometric element as the NURBS order in constant. Therefore, the next mesh ($h = 2$) has

$\Xi_2 = \{0,0,0,1/2,1,1,1\}$ knot vector and as forth. Figure 4 and Figure 5 show the relative estimation tolerance of IGA method for the h-refinement technique for quadratic and cubic NURBS, respectively. Results shows the increasing accuracy of IGA method of quadratic functions for fifth element bisection ($h = 32$) with 0.1% estimation error. In the case of cubic NURBS basis-functions, we get the required accuracy with lower number of IGEs. In addition, cubic NURBS has high accuracy for high vibration modes.
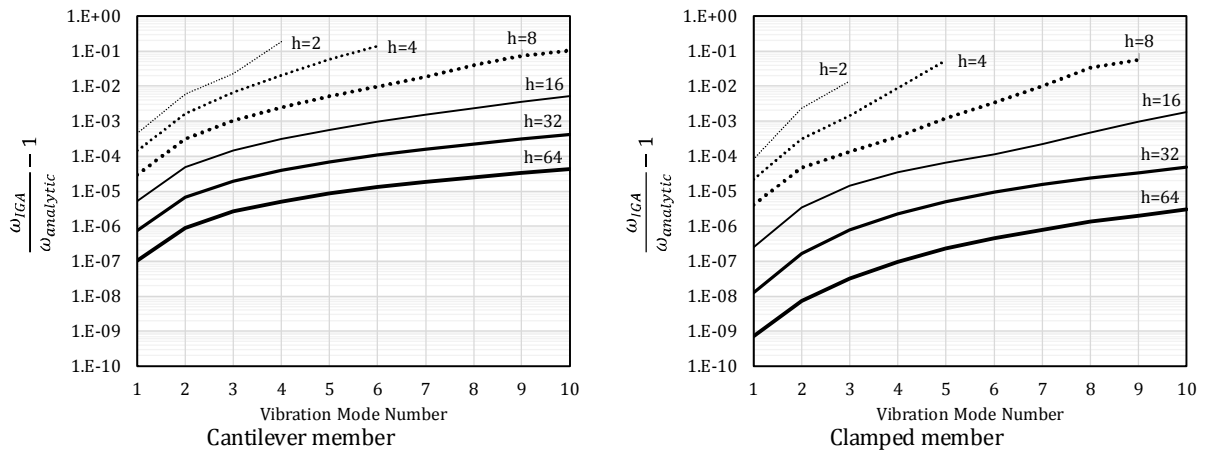

Fig 5: Relative estimation error for cubic NURBS in h-refining

In advance, we will measure the enhanced k-refinement technique on the convergence rate of frequency values to the exact ones in IGA method. Similar to the previous case, we start with single a quadratic ($k = 1$) NURBS element with $\Xi_1 = \{0,0,0,1,1,1\}$ knot vector. However, element is refined in NURBS order and knot insertion. Therefore, the next refining has $\Xi_2 = \{0,0,0,0,0.5,1,1,1,1\}$ knot vector ($k = 2$) and so forth. It should be noted that the number of control points is $n_{el} + p$ in a uniform IGA mesh, where n_{el} is the number of elements. Below is the obtained result using k-refinement technique to compare with the h-refinement method.
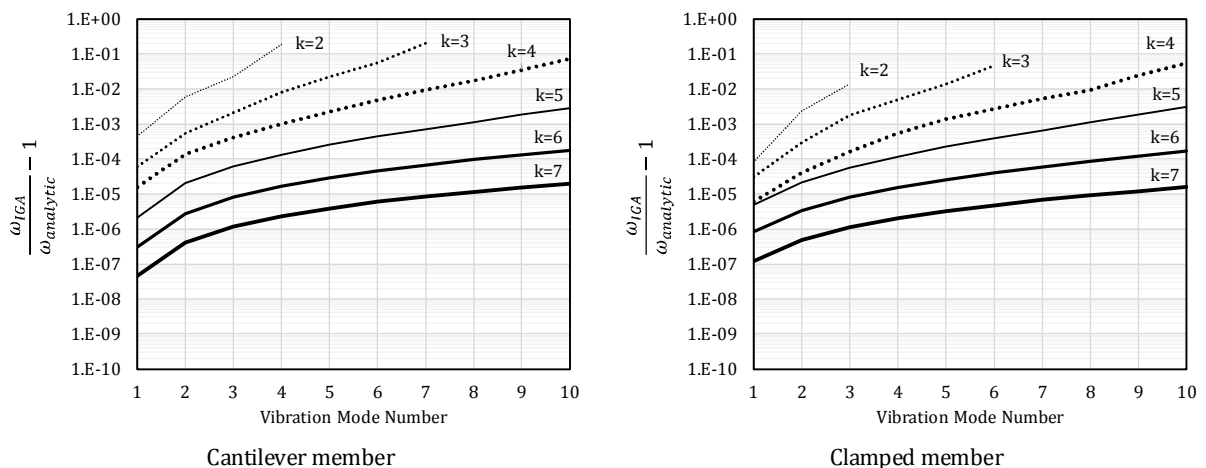

**Fig 6:** Relative estimation error for k-refining technique

154

Figure 6 shows the results obtained for vibration frequency calculation using k-refinement in IGA. As shown in figure, both clamped and cantilever member cases have the same sensitivity to the mesh refinement in k-refinement for high degree of freedom, dislike the h-refinement case. However, both h- and k-refinement methods obey the analogous variation with respect to the vibration mode. Comparison of abovementioned refining methods shows that k-refinement is suitable for the rest of dynamic analysis procedure, regardless of the study case. In addition, we have lower degrees of freedom in k-refinement technique than h-refinement, which speeds up the calculation process in advance. The authors select the ultimate mesh reached in vibration analysis ($k = 7$) with 1×10^{-5} relative estimation error to acquire the transient analysis results.

3.2. Transient analysis

Now we investigate the characteristics of the dynamic response of member modeled using IGA approach. For this purpose, we use the force excitation with uniform distribution along the member length. The force magnitude (F_0) is 10 N/mm and has the Dirac-delta ($\delta(t)$) impulsive time history. Such an excitation is appropriate for the vibration problems since we need to suppress the effect of the loading period. We have extracted the time-history of the displacement record at the free-end of the cantilever member and in the mid-span location of the clamped member. In order to simplify the results and further discussion, we have plotted the response and the frequency content of the related record using Fast Fourier Transform (FFT) spectrum in Figure 7. Fast Fourier transform (FFT) measures the natural oscillation frequencies of structures and is a frequency-based transform widely used in analysis of linear systems. It decomposes a signal into sine waves of different frequencies, which sum to the original waveform, distinguishing different frequency sine waves and their respective amplitudes. FFT is of great importance to signal processing. It used to extract the frequency content of structures and to detect damage in beams. The continuous FFT is as Eq. (25):

$$F(\omega) = \int_{-\infty}^{+\infty} f(t) exp(-i\omega t) dt \tag{25}$$

Functions as $f(t)$ and $F(\omega)$ denote given signal in time domain and Fourier transform in frequency domain. In structural health monitoring (SHM) theories, which exists in Farrar and Worden [26], Chang and Liu [27] and Chen *et al*. [28] works, the response due to excitation used for response detection is linear although the properties of geometry change. However, here features of system during transient and steady states responses are decomposed to characterize response, which is currently active. In other words, although FFT tentatively is used for whole time-history assessment, evaluation of frequencies and the affectivity of damping be measured. Still the Fourier transform cannot determine the information variations along time domain. For instance, if there is a local oscillation representing a particular phenomenon occurring within response time domain, its location is not recognized. The latter case is the non-stationary signal, which the frequencies alter over time. Primarily we assumed an ideal system without energy dissipation. Figure 7 shows both the record and the amplitude spectrum.
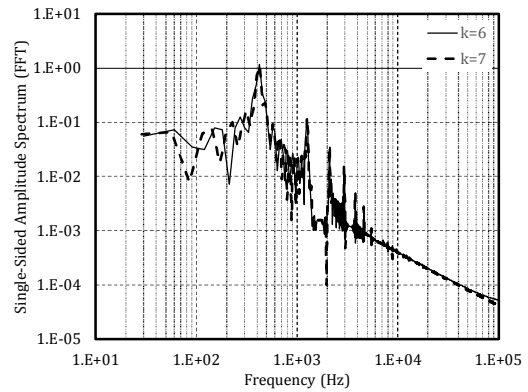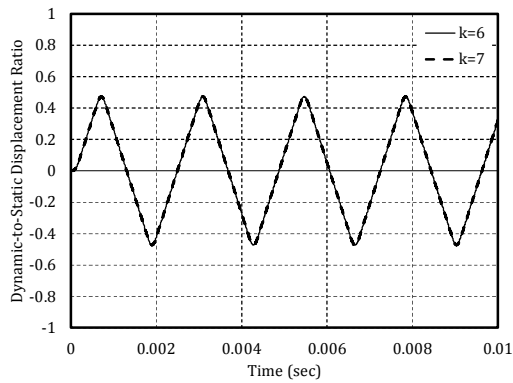
Excited Displacement History   FFT Analysis

Fig7: Un-damped oscillation of cantilever rod and the amplitude spectrum
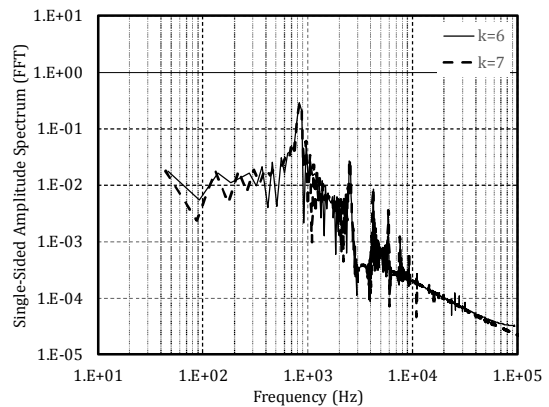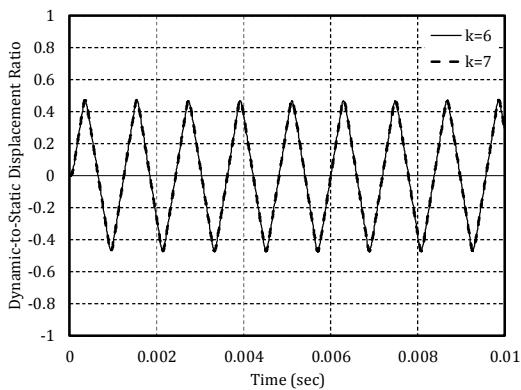
Excited Displacement History   FFT Analysis

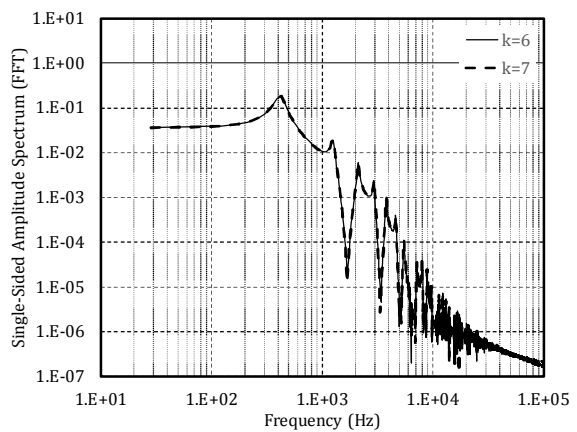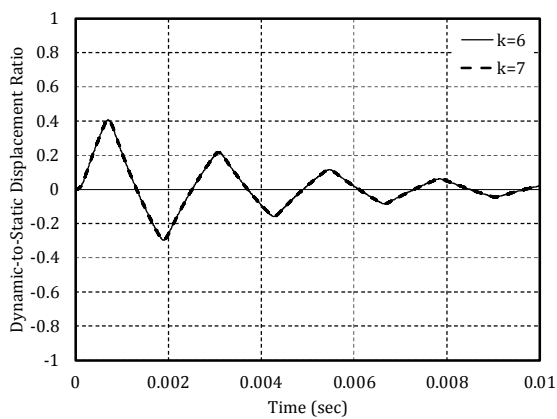**Fig 8:** Un-damped oscillation of clamped rod and the amplitude spectrum

Fig 9: Damped oscillation of cantilever rod and the amplitude spectrum

If one divides the amplitudes of each vibration frequencies to the static value, we acquire the modal participation factors as 82.2%, 8.9%, 2.7%, 1.1%, and 0.4% for the first, five modes. In advance, we select the clamped beam with the same impulsive force excitation. It should be noted that due to symmetry of the boundary conditions with respect to mid-span, the odd-number modes are excited. The modal participation factors are estimated as 85.3%, 8.0%, 2.6%, 1.1%, and 0.4%, for the first five modes using the FFT data as shown in Figure 8. The reduction in the peak FFT amplitude and increase in the corresponding frequency is notable. We acquire the analogous values using the closed form solution in analytical methods.
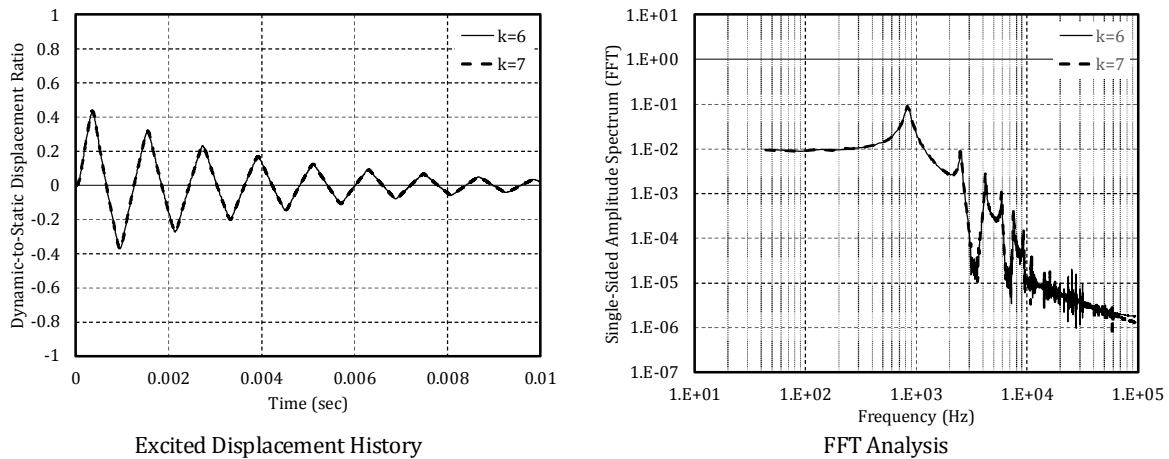

Excited Displacement History   FFT Analysis

Fig 10: Damped oscillation of clamped rod and the amplitude spectrum

Now, we go through the response characteristics of the damped case for both members. We assumed that the initial inherent viscosity of system (μ) is $4.15 \times 10^{-6}\ N \cdot s/mm^4$ [29]. Here, we do not use the proportional damping assumption since the modes other than the specified modes are over-damped or under-damped. The exact case is to determine the damping percentage of each mode using the FFT spectrum and frequency content. It is notable that the half-power bandwidth of the ith vibration mode is $2\xi_i$ at the $1/\sqrt{2}$ fraction of the resonant amplitude in spectrum. Therefore, we primarily present the oscillation of damped system and then extend the FFT analysis to measure the damping percentage of modes. It is useful to determine if each vibration mode has the same percentage or not and if so what is the pattern. Figure 9 shows the displacement time-history and the FFT spectrum of the cantilever member. In advance, Figure 10 shows that analogous results for clamped member. The logarithmic decrement of motion is as Eq. (26) for the determination of damping for the first mode.

$$\delta = \ln(u_i/u_{i+1}) = 2\pi\alpha/\sqrt{1-\alpha^2} \qquad (26)$$

Here, α is the damping percentage of first mode. If we replace the displacement of two successive waves in above equation, we will have the $\alpha = 10\%$ for the cantilever problem. In addition, we will have $\alpha = 5\%$ for the clamped case, respectively. However, for the wave damping analysis of other modes, we have to use the bandwidth method. Due to non-proportionality of the provided damping, the use of orthogonal-mode decomposition is not applicable. As the peak pulses of the FFT spectra are so narrow in the free-vibration plots, we acquire $\alpha = 0.0\%$ for un-damped case. Table 1 and Table 2 shows the damping percentage of first-ten modes of clamped and cantilever members. For comparison of the results, we do the

same analysis using *Abaqus* FEM code with a overkill meshing. We have modeled the members with linear two-node elements.

Table 1: Damping percentage of vibration modes for IGA analysis

Mode	1st	2nd	3rd	4th	5th	6th	7th	8th	9th	10th
Clamped	5.00%	2.50%	1.67%	1.25%	1.00%	0.83%	0.71%	0.63%	0.56%	0.50%
Cantilever	10.00%	3.33%	2.00%	1.43%	1.11%	0.91%	0.77%	0.67%	0.59%	0.53%

Table 2: Damping percentage of vibration modes for FEM analysis

Mode	1st	2nd	3rd	4th	5th	6th	7th	8th	9th	10th
Clamped	5.00%	2.50%	1.67%	1.25%	1.00%	0.83%	0.71%	0.62%	0.55%	0.50%
Cantilever	10.00%	3.33%	2.00%	1.43%	1.11%	0.91%	0.77%	0.66%	0.58%	0.52%

As shows in Tables 1 and 2, there is almost no difference between regular-mesh IGA and fine-mesh FEM results, which approves the efficiency of IGA method in damped dynamic problems. The FEM models have 10^3 times more degrees of freedom than the $k = 7$ IGA model. We get the equal results for the first mode as acquired previously by logarithmic decrement. For modes higher than the eighth mode, IGA method acquired higher damping percentage than FEM for high modes. The comparison of IGA and FEM results is plotted in Figure 11.
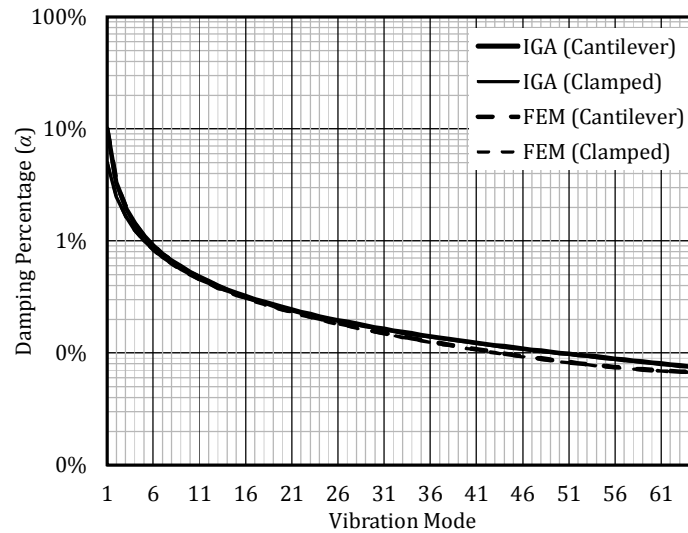

Fig 11: Damping percentage versus vibration mode calculated in IGA and FEM

We can conclude that the IGA method is quite accurate in modeling the vibration behavior of non-proportionally damped system with even lower degrees of freedom in discretized models. In addition, the FEM technique fails to determine the non-proportional damping of higher modes in comparison with IGA method. The IGA solution with k-refinement technique and the overkill FEM solution are not sensitive to the boundary conditions of problem. The FFT decomposition

combined with the IGA formulation are appropriate methods to determine the response characteristics of mechanical systems with inherent damping. For completion of the results, we present the energy time-history acquired by the IGA method. Primary validation is the conservative law of total energy. We can also determine the time-period required to dissipate the imposed energy. Figure 12 shows the time history of the system energies versus time.
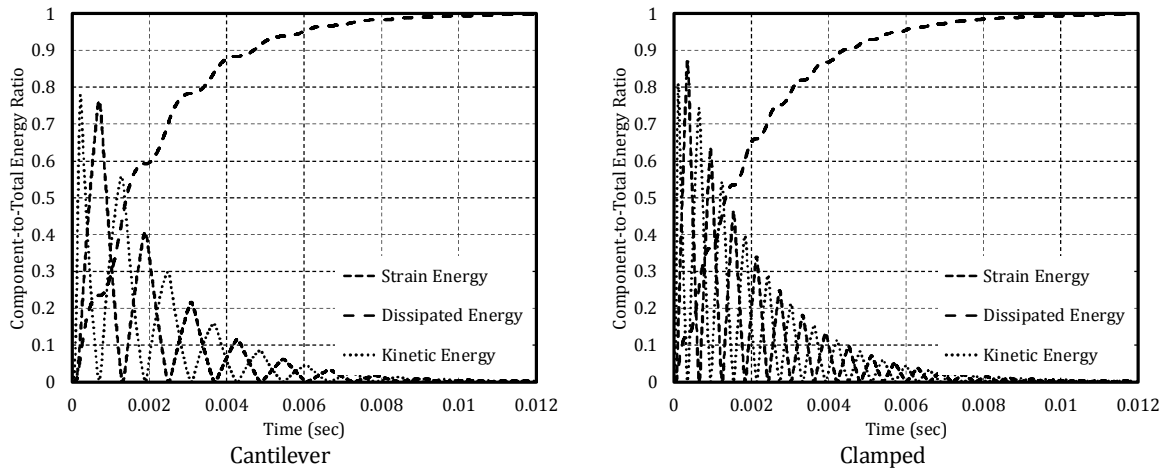

Fig 12: Integrated Energies versus time for IGA solution

We note that either clamped or cantilever member dissipate the impose energy in a same time which only depend on the inherent viscosity of material. Systems with higher vibration frequencies only required more oscillation to absorb the energy. For this special case, time to dissipate the total energy is 10 $msec$, which can also be calculated by the theoretical method. In addition, we will go through the wavelet decomposition to investigate the characteristics of vibration.

3.3. Continuous wavelet transformation

Kitada[30] expressed that the wavelet transform (WT) breaks a signal into shifted and scaled versions of the selected wavelet, called as basis function which are compact in both time and frequency domains. Basis functions should integrate to zero and be square integrable with finite energy level. Unlike the FFT method, the data on both time and frequency domain are maintained, depending on the scale-time range used in wavelet transformation. Here the time variable differentiates the simultaneous damages that happen at different locations for impact load. The continuous wavelet transformation (CWT) is as Eq. (27):

$$C(a,b) = \int\limits_{-\infty}^{+\infty} \frac{1}{\sqrt{a}} f(t) \varphi\left(\frac{t-b}{a}\right) dt \qquad (27)$$

Here, a and b parameters denote the scale and position of base function respectively over time. The CWT method captures the high frequency and high period oscillations for $a < 1$ and $a > 1$ scales in that order. Coefficients $W(a,b)$ represent the similarity correlation of the scaled wavelet to specific section of response signal. In this study, the Morlet wavelet is the mother wavelet with Eq. (28) definition, which is efficient in damage crack assessment which is

159

presented in Liew and Wang[13] works. The selected base function with regular and square integrals are plotted in Fig 13 where the major part of excitation energy (square integral) is delimited to $|t| \leq 3.0$ sec time domain.

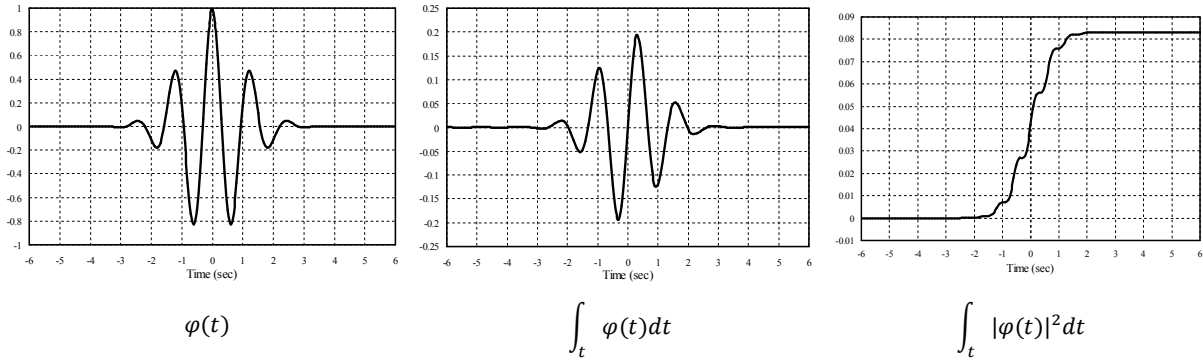$$\varphi(t) = exp\left(-\frac{t^2}{2}\right)cos(5t) \tag{28}$$

$\varphi(t)$ $\int_t \varphi(t)dt$ $\int_t |\varphi(t)|^2 dt$

Fig 13: Morlet wavelet time function supplied with regular and square integrals

The output of CWT analysis is a plot on which the x −axis represents position along the time domain (b), the y −axis represents scale (a), and the color at each $x − y$ point represents the magnitude of the wavelet coefficients, $W(a, b)$. The CWT coefficient plots are accurately the time-scale view of the response signal. It is a different view of extracted data and is relevant to the time-frequency FFT content. In the damage of beam impact, the natural frequency decreases as shear and flexural cracks propagate (Liew *et. al.*[31]). The decrease of frequency causes an increase of the wavelet scale and corresponding coefficient in the CWT. Therefore, the CWT analysis detects the damage-induced property alterations specifically. We present the wavelet analysis results for the un-damped and damped IGA solution in Figure 14 and Figure 15, respectively.
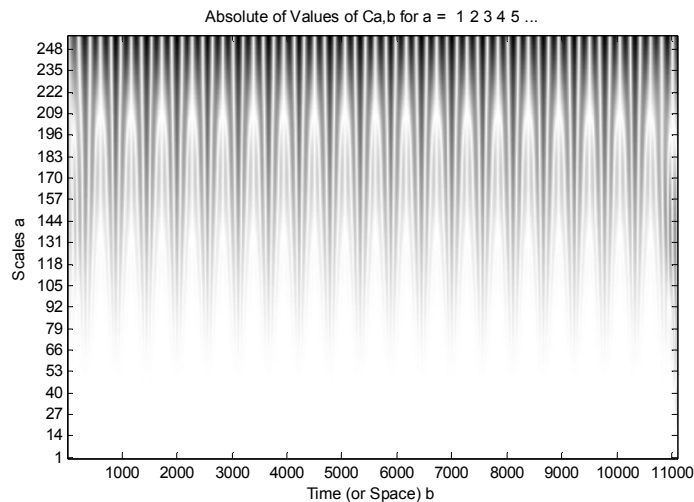

Fig 14: Coefficients of CWT versus scales of un-damped IGA solution (time in micro-sec)
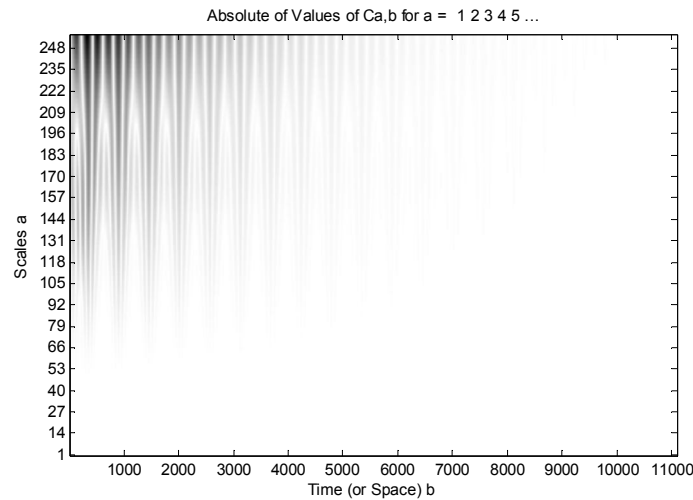
Fig 15: Coefficients of CWT versus scales of damped IGA solution (time in micro-sec)

For the un-damped case, we detect the participation the decreasing participation of high modes as the wavelet scale decreases. The coefficient distribution along time is constant for a definite scale which shows the stable oscillation of each period. For the damped case, results show that high-frequency modes have lower damping ratio than high-period modes. In addition, the participation ratio of each mode is decreasing over time. In this way, the CWT decomposition of IGA solutions has the complete correlation with the FFT analysis. We can measure the response of members with non-uniformly distributed material properties. Here, we assume the rod with $E(x) = E \sin(2\pi x/L)$ distribution for elastic modulus. In other words, we have two non-prismatic rod connected to each other in the mid-span location. We assume the clamped boundary condition for the problem. For a general analysis case we present both the un-damped and damped oscillation case with the k-refinement achieved in the previous sections. The loading history and the viscosity of the material are analogous to the previous cases. Figure 16 shows the time-history of the mid-span displacement and the FFT spectrum content.
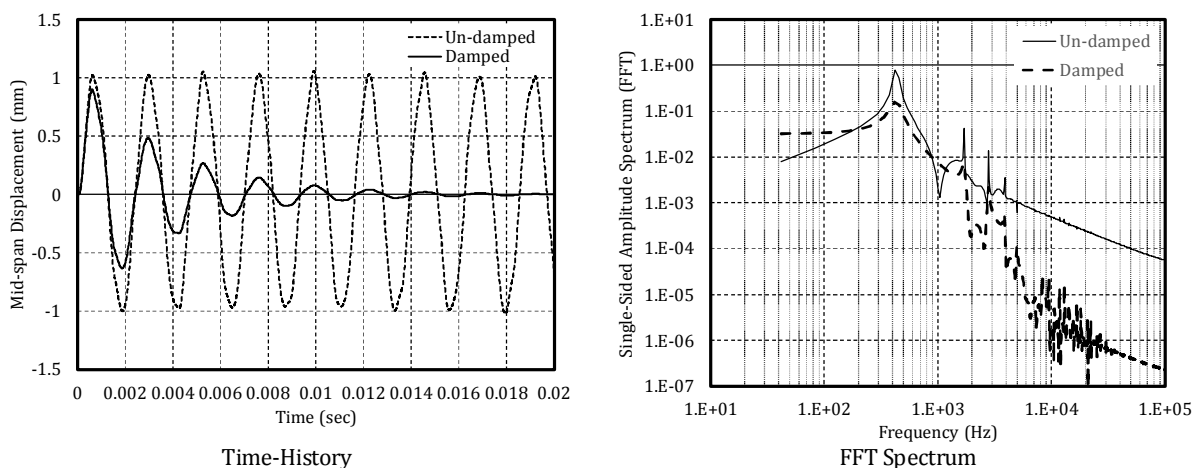

Time-History

FFT Spectrum

Fig 16: Oscillation of clamped non-prismatic rod and the amplitude spectrum

As shown in the above figure, several modes govern the vibration of both cases as rod rods are vibrating interactively. Using the half-power bandwidth method, we acquire 9.7%, 5.9%, 2.5%, 2.1% and 1.5% damping percentage for the first-five vibration modes. We detect that for non-prismatic member case, the damping ratio does not have sharp descending pattern for high modes. In other words, high-frequency modes have almost the same damping ratios. Although high-frequency modes are not present in oscillation of the un-damped case, there exist in the damped member with very small amplitudes as shown in the FFT spectrum.
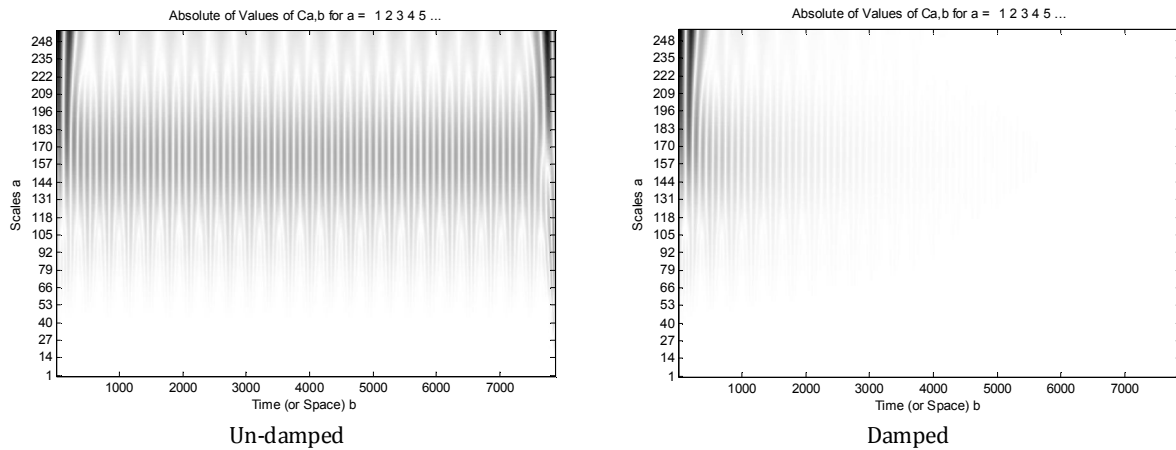

Un-damped

Damped

Fig 17: Coefficients of CWT for non-prismatic member in IGA solution (time in micro-sec)

The CWT spectrum of response is shown in Fig 17. We detect mid-range and high-range frequencies in un-damped response. Dislike the prismatic case, the first mode only governs the start of vibration and then high-frequency vibration is activated. For the damped case, the CWT spectrum shows non-uniform dissipation of energy between modes. Low- and high-frequencies have lower kinetic energies than the mid-range frequency mode. Since the IGA method captures the vibration modes exactly, the dynamic response evaluation within this method provides precious database.

4. Conclusion

Current study deals with the development of the isogeometric formulation for the one-dimension vibration problem. We measure the accuracy of the isogeometric analysis method using both closed-form and the overkill finite element method solutions. The h- and k-refinement techniques are used for mesh refining. Results consist of vibration frequency, time-history records, fast Fourier transform and wavelet spectra. We use the mentioned decomposition method to determine the characteristics of the assessed dynamic response. We make following outcomes based on the results:

- The k-refinement technique has enhanced the accuracy convergence with respect to the h-refinement method both in modal and time-history procedures.

- The half-power bandwidth method gives the effective damping percentage of the vibration modes for the IGA solution with appropriate accuracy with respect to FEM method.

162

- Meshing convergence ratio is fast in the IGA method with respect to classical FEM solution. The accuracy difference between quadratic and cubic NURBS is significant in h-refinement technique of IGA solution.

- The FEM method underestimates the damping ratios of the high-frequency modes in compare with the IGA method.

- CWT used for decomposition of results show that the participation of high-frequency mode decrease with respect to the high-period modes along time.

Refrences

[1] T.J.R. Hughes, J.A. Cottrell, Y. Bazilevs, Isogeometric analysis: CAD, finite elements, NURBS, exact geometry and mesh refinement, Computer methods in applied mechanics and engineering, 194 (2005) 4135-4195.

[2] C. Boor, A Practical Guide to Splines, Springer-Verlag New York, 1978.

[3] J.A. Cottrell, T.J.R. Hughes, Y. Bazilevs, Isogeometric analysis: toward integration of CAD and FEA, John Wiley & Sons, 2009.

[4] A. Buffa, G. Sangalli, R. Vázquez, Isogeometric analysis in electromagnetics: B-splines approximation, Computer Methods in Applied Mechanics and Engineering, 199 (2010) 1143-1152.

[5] M.H. Aigner, Ch. Heinrich, C., Jüttler, B., Pilgerstorfer, E., Simeon, B., Vuong, A.-V, Swept volume parametrization for isogeometric analysis, In: Hancock, E., Martin, R. (Eds.), The Mathematics of Surfaces. MoS XIII, 2009 Springer., (2009).

[6] T.J.R. Hughes, A. Reali, G. Sangalli, Efficient quadrature for NURBS-based isogeometric analysis, Computer methods in applied mechanics and engineering, 199 (2010) 301-313.

[7] Y. Bazilevs, V.M. Calo, T.J.R. Hughes, Y. Zhang, Isogeometric fluid-structure interaction: theory, algorithms, and computations, Computational mechanics, 43 (2008) 3-37.

[8] Y. Bazilevs, V.M. Calo, J.A. Cottrell, J.A. Evans, T.J.r.R. Hughes, S. Lipton, M.A. Scott, T.W. Sederberg, Isogeometric analysis using T-splines, Computer Methods in Applied Mechanics and Engineering, 199 (2010) 229-263.

[9] M.R. Dörfel, B. Jüttler, B. Simeon, Adaptive isogeometric analysis by local h-refinement with T-splines, Computer methods in applied mechanics and engineering, 199 (2010) 264-275.

[10] S. Lipton, J.A. Evans, Y. Bazilevs, T. Elguedj, T.J.R. Hughes, Robustness of isogeometric structural discretizations under severe mesh distortion, Computer Methods in Applied Mechanics and Engineering, 199 (2010) 357-373.

[11] V.P. Nguyen, C. Anitescu, P.A. Bordas, T. Rabczuk, Isogeometric analysis: an overview and computer implementation aspects, Mathematics and Computers in Simulation, 117 (2015) 89-116.

[12] T.J.R. Hughes, A. Reali, G. Sangalli, Duality and unified analysis of discrete approximations in structural dynamics and wave propagation: comparison of p-method finite elements with k-method NURBS, Computer methods in applied mechanics and engineering, 197 (2008) 4104-4124.

[13] D. Wang, W. Liu, H. Zhang, Novel higher order mass matrices for isogeometric structural vibration analysis, Computer Methods in Applied Mechanics and Engineering, 260 (2013) 92-108.

[14] C.H. Thai, H. Nguyen-Xuan, N. Nguyen-Thanh, T.H. Le, T. Nguyen-Thoi, T. Rabczuk, Static, free vibration, and buckling analysis of laminated composite Reissner–Mindlin plates using NURBS-based isogeometric approach, International Journal for Numerical Methods in Engineering, 91 (2012) 571-603.

[15] O. Weeger, U. Wever, B. Simeon, Isogeometric analysis of nonlinear Euler–Bernoulli beam vibrations, Nonlinear Dynamics, 72 (2013) 813-835.

[16] S. Shojaee, E. Izadpanah, N. Valizadeh, J. Kiendl, Free vibration analysis of thin plates by using a NURBS-based isogeometric approach, Finite Elements in Analysis and Design, 61 (2012) 23-34.

[17] L.V. Tran, A.J.M. Ferreira, H. Nguyen-Xuan, Isogeometric analysis of functionally graded plates using higher-order shear deformation theory, Composites Part B: Engineering, 51 (2013) 368-383.

[18] C.H. Thai, A.J.M. Ferreira, E. Carrera, H. Nguyen-Xuan, Isogeometric analysis of laminated composite and sandwich plates using a layerwise deformation theory, Composite Structures, 104 (2013) 196-214.

[19] P. Phung-Van, M. Abdel-Wahab, K.M. Liew, S.P.A. Bordas, H. Nguyen-Xuan, Isogeometric analysis of functionally graded carbon nanotube-reinforced composite plates using higher-order shear deformation theory, Composite structures, 123 (2015) 137-149.

[20] F. Tornabene, N. Fantuzzi, M. Bacciocchi, A new doubly-curved shell element for the free vibrations of arbitrarily shaped laminated structures based on Weak Formulation IsoGeometric Analysis, Composite Structures, 171 (2017) 429-461.

[21] T. Yu, S. Yin, T. Bui, S. Xia, S. Tanaka, S. Hirose, NURBS-based isogeometric analysis of buckling and free vibration problems for laminated composites plates with complicated cutouts using a new simple FSDT theory and level set method, Thin-Walled Structures, 101 (2016) 141-156.

[22] N. Fantuzzi, G. Della Puppa, F. Tornabene, M. Trautz, Strong Formulation IsoGeometric Analysis for the vibration of thin membranes of general shape, International Journal of Mechanical Sciences, 120 (2017) 322-340.

[23] S. Yin, T. Yu, T. Bui, P. Liu, S. Hirose, Buckling and vibration extended isogeometric analysis of imperfect graded Reissner-Mindlin plates with internal defects using NURBS and level sets, Computers & Structures, 177 (2016) 23-38.

[24] L. Dedè, C. Jäggli, A. Quarteroni, Isogeometric numerical dispersion analysis for two-dimensional elastic wave propagation, Computer Methods in Applied Mechanics and Engineering, 284 (2015) 320-348.

[25] MATLAB 7.04 User's Manual., MathWorks, USA., 2005.

[26] C.R.W. Farrar, K., An introduction to structural health monitoring, Philosophical Transactions of the Royal Society of London A, Mathematical, Physical and Engineering Sciences, 365 (2007) 303-315.

[27] P.C. Chang, S.C. Liu, Recent research in nondestructive evaluation of civil infrastructures, Journal of materials in civil engineering, 15 (2003) 298-304.

[28] S.L. Chen, H.C. Lai, K.C. Ho, Identification of linear time varying systems by Haar wavelet, International journal of systems science, 37 (2006) 619-628.

[29] ASTM, A568-Standard, "Specification for Steel Sheet, Carbon, and High Strength Low-Alloy, Hot-Rolled and Cold-Rolled".

[30] Y. Kitada, Identification of nonlinear structural dynamic systems using wavelets, Journal of Engineering Mechanics, 124 (1998) 1059-1066.

[31] K.M. Liew, Q. Wang, Application of wavelet theory for crack identification in structures, Journal of engineering mechanics, 124 (1998) 152-157.